www.czasopisma.pan.pl PAN www.journals.pan.pl
ARCHIVES OF ACOUSTICS Vol. 47, No. 2, pp. 151–167 (2022), doi: 10.24425/aoa.2022.141646

Research Paper

Microphone Based Acoustic Vector Sensor for Direction Finding with Bias Removal

Mohd WAJID[(1),(2)*], Arun KUMAR[(2)], Rajendar BAHL[(2)]

[(1)] *Department of Electronics Engineering, Z.H.C.E.T.*
Aligarh Muslim Univesity
Aligarh, India

[(2)] *Centre for Applied Research in Electronics,*
Indian Institute of Technology Delhi
New Delhi, India
*Corresponding Author e-mail: wajidiitd@ieee.org

(*received May 22, 2020; accepted March 10, 2022*)

The acoustic vector sensor (AVS) is used to measure the acoustic intensity, which gives the direction-of-arrival (DOA) of an acoustic source. However, while estimating the DOA from the measured acoustic intensity the finite microphone separation (d) in a practical AVS causes angular bias. Also, in the presence of noise there exists a trade off between the bias (strictly increasing function of d) and variance (strictly decreasing function of d) of the DOA estimate. In this paper, we propose a novel method for mitigating the angular bias caused due to finite microphone separation in an AVS. We have reduced the variance by increasing the microphone separation and then removed the bias with the proposed bias model. Our approach employs the finite element method (FEM) and curves fitting to model the angular bias in terms of microphone separations and frequency of a narrowband signal. Further, the bias correction algorithm based on the intensity spectrum has been proposed to improve the DOA estimation accuracy of a broadband signal. Simulation results demonstrate that the proposed bias correction scheme significantly reduces the angular bias and improves the root mean square angular error (RMSAE) in the presence of noise. Experiments have been performed in an acoustic full anechoic room to corroborate the effect of microphone separation on DOA estimation and the efficacy of the bias correction method.

Keywords: acoustic measurements; acoustic sensor; acoustic vector sensor; direction-of-arrival estimation; finite element analysis; microphones; particle velocity; sound source localization.

1. Introduction

The finite microphone separation and sensor noise in an acoustic vector sensor (AVS) cause a systematic error (bias) and random error (variance) in the acoustic intensity measurement respectively, thereby, inaccurate direction-of-arrival (DOA) estimate. In this paper, we have proposed the non-linear modelling of the bias caused by microphone separation as well as signal frequency. Also, acoustic intensity based bias free estimation of DOA for the narrowband as well as broadband signals is devised. The bias model also helps in reducing the variance of DOA caused by the sensor noise.

The acoustic intensity is a measure of the rate of flow of energy per time unit and per area unit (normal to the direction of energy flow) by an acoustic wave (WIEDERHOLD *et al.*, 2012). It is a vector quantity useful for determining and characterising various parameters of the acoustic field including the DOA of sound from a source if a single source is present in the field. The direction of the acoustic intensity is the same as the direction of energy flow from an acoustic source at the measurement location. Mathematically, the acoustic intensity at any point is defined as the product of the pressure and the particle velocity at that point in space (DALL'OSTO, DAHL, 2015). In recent years, researchers have focused on AVS

based intensity measurement and its use in DOA estimation of acoustic sources (Kotus, 2012; 2015; Kotus, Czyżewski, 2010; Kotus *et al.*, 2014; 2016; Kotus, Kostek, 2015; Odya *et al.*, 2017; Wajid, Kumar, 2020). There are mainly two techniques for calculating acoustic intensity: one of them is based on P-P (pressure-pressure) method and the other is based on the P-U (pressure-velocity) method. In the P-P method, the particle velocity component is derived from the measured signals of two closely separated microphones while in the P-U method, the particle velocity is measured directly or derived from an accelerometer measurement (Jacobsen, 2014; Jacobsen, de Bree, 2005). Also, there are commercial probes available for P-U method which directly measure pressure and particle velocity using two tiny platinum wires. This P-U sensor is based on thermal imbalance caused by particle velocity (de Bree, 2003; de Bree *et al.*, 2001; Raangs *et al.*, 2003). The P-P method is reported to be more robust under the considerable non-acoustic temperature and velocity fluctuations (Giraud *et al.*, 2010; Jacobsen, n.d.; Thomas *et al.*, 2015). However, the P-P method suffers from bias in DOA estimation due to microphone separation and frequency dependent phase and gain mismatch of microphones. The microphone separations define the limit on the highest measurement frequency of the acoustic signal, and their microphones' gain and phase mismatch set the lower limit of the frequency of the signal. The P-P method underestimates the acoustic intensity when the microphone separation reaches up to half of the wavelength (spatial Nyquist frequency) (Shirahatti, Crocker, 1992). In the P-P method, finite difference (FD) approximation of the pressure gradient of the sound field is used to derive the acoustic particle velocity component. In FD approximation, the separation d between acoustic centres of the microphones need to be much smaller than the wavelength λ of the acoustic source. The FD approximation errors become smaller by reducing the values of d/λ and d/r, where r is the distance of the acoustic source from the AVS (Fahy, 1977; Thompson, Tree, 1981). Inaccuracies in the estimated pressure gradient in the P-P method increase as the wavelength approaches the Nyquist limit in spatial frequency. Also at larger wavelengths, the pressure difference between the microphone's measurements will be smaller, which can be easily corrupted by the noise and cause an error in the pressure gradient approximation, and thereby, the acoustic intensity (Bai *et al.*, 2013; Miah, Hixon, 2010). In addition to the P-P and P-U based vector sensor, there are other direction sensors known as ambisonic microphones (also called SoundField microphone) which can capture sound fields from 360° space (in addition to the horizontal plane, it captures sound fields from above and below the listener plane). The ambisonic sensor consists of four directional microphones with cardioid beam patterns, these directional microphones are placed on the tetrahedral surface pointing in four different outward directions. So it captures four channel acoustic signals, namely, right back (RB) signal, right front (RF) signal, as well as left front (LF) signals and left-back (LB) signals. The linear combination of these captured signals will generate the directional patterns (figure-of-eight) along the x-axis, y-axis, and z-axis, known as a B-format recording. The three orthogonal directional patterns resemble the directional components of the pressure gradient. However, in our study, we have used only omnidirectional microphones which are closely spaced to provide directional characteristics with low cost.

Cazzolato and Hansen (2000) have derived the error expression using the P-P method in estimating mid-point pressure, particle velocity and acoustic energy density due to microphone separation and its gain and phase mismatch. They have observed that for a plane progressive wave, the normalised error in particle velocity estimate is less than the normalised error in the mid-point pressure estimate for the given frequency and microphone separation. The noise statistics for the particle velocity estimated using isotropic sensors have been derived by Olenko and Wong (2013; 2015). However, its effect on the DOA estimation of the acoustic source has not been discussed. Also, they have not considered the effect of separation of isotropic sensors and its effect on SNR for the estimated particle velocity. Thomas *et al.* (2015) have proposed a phase and amplitude gradient method for estimating the acoustic vector quantity which does not produce frequency-dependent bias inherent due to microphone separation. Jacobson *et al.* (1998) have investigated the acoustic intensity measurement performance at high frequency through numerical and experimental investigations. They have concluded that the optimum length of the spacer between the microphones is equal to the diameter of the microphone. The FD error with this spacer size will counterbalance the effect of diffraction for the signal frequencies below the frequency limit, which is twice of the frequency limit set by FD approximation. However, they have considered only two microphone probes, which gives an intensity component only along the line joining the two microphones in a probe. Parkins *et al.* (2000) have presented analytical results, simulation and experimental results on the error in the measurement of energy density and intensity using two different vector field configurations (six microphones mounted on the surface of a hard sphere – referred to as a spherical sensor and freely suspended microphone configuration). It has been suggested that a spherical sensor is more accurate, however, the effective microphone separation increases due to diffraction in the case of a spherical sensor. Wiederhold *et al.* (2012; 2014) have also given a detailed analysis on intensity and its direction

measurement for "freely suspended orthogonal microphones" and "orthogonal microphones embodied on the hard spherical surface". Hickling and Brown (2011) have taken regular tetrahedron configuration for the estimation of sound intensity and direction. However, the results for DOA estimation error are not given in detail and microphone separation bias is not discussed. The direction finding based on the eigendecomposition of the data matrix of different "pressure and uniaxial particle velocity sensor" configurations have been derived (Song *et al.*, 2015). However, they have used prior information about the interval of source location and spacing between the sensors. Also, they have used model of ideal particle velocity sensor, and the effect of microphone separation within a particle velocity sensor has not been considered, and the accuracy of DOA estimate is not discussed. Different configurations of biaxial particle velocity sensors (two uniaxial particle velocity sensors are differently oriented and spatially separated) have been investigated for direction finding (Song *et al.*, 2015). However, it requires prior information regarding the source incident sector. Song and Wong (2015) have derived DOA for the particle velocity sensors triad, where particle velocity sensors are orthogonally oriented and spread arbitrarily in the space. They have used the ideal model of particle velocity sensor and used an eigen-based DOA estimate which might be computationally complex due to the calculation of covariance matrix and its decomposition. Also, larger separations between sensors are required for better resolution. Wong and Zoltowski (1997) have given aperture extension of a uniform rectangular array of vector sensors where vector sensors can be spaced more than half-wavelength. They have proposed a subspace based technique algorithm for DOA estimation. Zoltowski and Wong (2000) have also used the subspace technique on an array of vector sensors. They have tried to reduce the directional ambiguity caused due to larger sensor separation. However, they have used the model of ideal particle velocity sensors. Lee *et al.* (2016) have discussed the effect of the non-orthogonal arrangement of the biaxial velocity sensor on the pointing error in its beamformer.

In most of the existing studies discussed above, the particle velocity, acoustic intensity, and sound power have been considered for error analysis for the P-P based vector sensor configurations. In this paper, we have analysed the effects of microphone separation, source signal frequency, and signal-to-noise ratio (SNR) on DOA estimation. We give an estimate of the DOA bias of the acoustic source using acoustic intensity measured with the P-P method. The three microphone based AVS configuration in which microphones are placed at the vertices of an equilateral triangle (named as delta configuration) is used for acoustic intensity computation and hence DOA estimation. We have considered delta configuration because it had been proved to be the best three microphone configuration amongst other possible three microphone configurations for DOA estimation in the presence of noise (Wajid *et al.*, 2016). It has been assumed that all the microphones are identical, of negligible size and possess omni-directional beam pattern. Also, there is no imbalance between the microphone channels, and the AVS is located in the far-field of the source. We have proposed a bias correction scheme of DOA estimate that is attributed to microphone separation and frequency of the acoustic signals. The proposed correction term has been studied for different SNR values in the presence of correlated and uncorrelated noise field. The proposed method of bias correction can also be applied to any DOA estimation algorithms which are sensitive to microphone separations.

The remaining part of the paper is organised as follows: Sec. 2 describes the method of acoustic intensity based DOA estimation using FD approximation of the pressure gradient, Sec. 3 gives a DOA estimator for the delta configuration of an AVS along with the quantitative estimate of the bias. Section 4 presents the finite element method (FEM) simulation, proposes the bias model for DOA estimation of a narrowband signal, and presents the performance of the bias correction scheme in the presence of noise. Section 5 proposes the algorithm for bias correction of DOA estimate for broadband signals. Section 6 is related to anechoic room experimentation for different microphone separations. Finally, Sec. 7 gives conclusions about the work done.

2. The acoustic intensity and DOA estimation

This section is devoted to a brief mathematical background of DOA estimation using acoustic intensity which is derived from the spatial sampling of the pressure field. Also, the performance evaluation parameters of DOA estimation are defined in this section.

The instantaneous acoustic intensity is a function of pressure and particle velocity whose components along the x-axis (the line connecting the two microphones) is defined as

$$I_x(t) = p_x(t)v_x(t), \tag{1}$$

where $p_x(t)$ and $v_x(t)$ are realisations of the jointly stationary processes of pressure and particle velocity, respectively. The time average intensity is given by

$$I_x = \langle p_x(t)v_x(t)\rangle = R_{p_x v_x}(0), \tag{2}$$

where $R_{p_x v_x}(\tau)$ represents the cross-correlation function between the $p_x(t)$ and $v_x(t)$ at delay τ. The time average intensity component, I_x, can be written in terms of cross power spectral density between pressure and particle velocity signals. The inverse Fourier transform of the cross power spectral density $S_{p_x v_x}(\omega)$

is the cross-correlation function (Chung, 1978; Fahy, 1977; Gade, 1982), therefore:

$$R_{p_x v_x}(\tau) = \int_{-\infty}^{\infty} S_{p_x v_x}(\omega) \cdot e^{j\omega\tau}\, \mathrm{d}\omega. \tag{3}$$

If $R_{p_x v_x}(\tau)$ is a real valued function then we have:

$$I_x = R_{p_x v_x}(0) = \int_{-\infty}^{\infty} \mathrm{Re}\left[S_{p_x v_x}(\omega)\right] \mathrm{d}\omega. \tag{4}$$

Considering the FD approximation of the pressure gradient for finding the particle velocity $v_x(t)$ as defined below:

$$\widehat{v}_x(t) \backsimeq -\frac{1}{\rho_o} \int_{-\infty}^{t} \frac{p_2(\tau) - p_1(\tau)}{d}\, \mathrm{d}\tau, \tag{5}$$

where ρ_o is the mass density of the medium. Assuming the pressure signal at a point location as the arithmetic mean of the measured pressure signal $p_1(t)$ and $p_2(t)$ at the two microphones, which is given by

$$\widehat{p}_x(t) = \frac{1}{2}\left[p_1(t) + p_2(t)\right], \tag{6}$$

the Fourier transform of Eqs (5) and (6) are

$$\widehat{V}_x(\omega) = -\frac{1}{\rho_o d}\frac{1}{j\omega}\left[P_2(\omega) - P_1(\omega)\right] \tag{7}$$

and

$$\widehat{P}_x(\omega) = \frac{1}{2}\left[P_1(\omega) + P_2(\omega)\right], \tag{8}$$

respectively. The estimate of cross power spectrum $\widehat{S}_{\widehat{p}_x\widehat{v}_x}(\omega)$ is given by

$$\widehat{S}_{\widehat{p}_x\widehat{v}_x}(\omega) \triangleq E\left[\widehat{P}_x^*(\omega)\widehat{V}_x(\omega)\right]. \tag{9}$$

If $\widehat{p}(t)$ and $\widehat{v}_x(t)$ are real valued function then

$$\begin{aligned}\widehat{S}_{\widehat{p}_x\widehat{v}_x}(\omega) &= \widehat{S}^*_{\widehat{v}_x\widehat{p}_x}(\omega) \\ &= \frac{j\left[S^*_{p_2p_2}(\omega) - S^*_{p_1p_1}(\omega)\right] - 2\,\mathrm{Im}\left[S_{p_1p_2}(\omega)\right]}{2\rho_o\omega d},\end{aligned} \tag{10}$$

where $S_{p_1p_1}(\omega)$ and $S_{p_2p_2}(\omega)$ are the power spectral density of $p_1(t)$ and $p_2(t)$, respectively, and $S_{p_1p_2}(\omega)$ is the cross power spectral density between $p_1(t)$ and $p_2(t)$. Taking the real part of $\widehat{S}_{\widehat{p}_x\widehat{v}_x}(\omega)$, we get

$$\mathrm{Re}\left[\widehat{S}_{\widehat{p}_x\widehat{v}_x}(\omega)\right] = \left(-\frac{1}{\rho_o\omega d}\right)\mathrm{Im}\left[S_{p_1p_2}(\omega)\right]. \tag{11}$$

Using Eqs (4) and (11), the intensity along the x-axis is estimated as

$$\widehat{I}_x = -\frac{1}{\rho_o d}\int_{-\infty}^{\infty} \frac{1}{\omega}\,\mathrm{Im}\left[S_{p_1p_2}(\omega)\right] \mathrm{d}\omega. \tag{12}$$

Therefore, the time average intensity component has been expressed in terms of cross-spectra of the pressure signals (Fahy, 1977; Gade, 1982). Similarly, the time average intensity component, I_y, along the y-axis can be estimated. The DOA with respect to y-axis and in clockwise direction for the single source can be expressed as the arc-tangent of the ratio of the two orthogonal intensity components as given below:

$$\widehat{\theta} = \tan^{-1}\left(\frac{\widehat{I}_x}{\widehat{I}_y}\right), \tag{13}$$

and the estimate of unit vector $\widehat{\mathbf{u}}$ pointing to the acoustic source is

$$\widehat{\mathbf{u}} = \frac{\widehat{I}_x + j\widehat{I}_y}{\sqrt{\widehat{I}_x^2 + \widehat{I}_y^2}}. \tag{14}$$

For determining the DOAs of multiple sources with disjoint spectrum, the different frequency bands of the intensity spectrum, $\widehat{I}_{x,\omega}$ (Eq. (15)), are used:

$$\widehat{I}_{x,\omega} = -\frac{1}{\rho_o d}\frac{1}{\omega}\,\mathrm{Im}\left[S_{p_1p_2}(\omega)\right], \tag{15}$$

therefore:

$$\widehat{I}_x = \int_{-\infty}^{\infty} \widehat{I}_{x,\omega}\, \mathrm{d}\omega. \tag{16}$$

When the microphones are not orthogonally arranged (as in delta configuration), projections of acoustic intensity on the orthogonal axes can be used to determine the average orthogonal intensity components (Shi, 2015; Wajid *et al.*, 2016). The accuracy of the DOA results is evaluated in terms of the angular error (AE) and root mean square angular error (RMSAE), as given below:

$$\mathrm{AE} = \frac{1}{N}\sum_{i=1}^{N} \cos^{-1}(\mathbf{u}^{\mathrm{T}}\widehat{\mathbf{u}}_i), \tag{17}$$

and

$$\mathrm{RMSAE} = \sqrt{\frac{\sum_{i=1}^{N}\left\{\cos^{-1}(\mathbf{u}^{\mathrm{T}}\widehat{\mathbf{u}}_i)\right\}^2}{N}}, \tag{18}$$

where $\mathbf{u}$ is the vector of unit magnitude pointing to the acoustic source, $\widehat{\mathbf{u}}_i$ is the estimate of $\mathbf{u}$ at the i-th realization, $(.)^{\mathrm{T}}$ indicates transpose, and N is the total number of independent realisations with additive noise taken at the microphone. The average performance over all angular locations is represented in terms of $\overline{\mathrm{AAE}}$ and $\overline{\mathrm{RMSAE}}$, which are defined as

$$\overline{\mathrm{AAE}}_{mk_1:m:mk_2} = \frac{1}{k_2 - k_1 + 1}\sum_{k=k_1}^{k_2} \left|\mathrm{AE}(mk)\right|, \tag{19}$$

and

$$\overline{\mathrm{RMSAE}}_{mk_1:m:mk_2} = \frac{1}{k_2 - k_1 + 1}\sum_{k=k_1}^{k_2} \mathrm{RMSAE}(mk), \tag{20}$$

where the argument mk represents the DOA of an acoustic source in degrees, and subscripts "$mk_1 : m : mk_2$" of $\overline{\text{AAE}}$ and $\overline{\text{RMSAE}}$ indicate the range of angles used for averaging over the different angular locations of the source with an increment of m degrees for different integers k_1 and k_2 (Wajid *et al.*, 2016).

3. DOA estimation for delta configuration and quantification of bias

The delta configuration of an AVS consists of three identical omni-directional microphones kept at the vertices of an equilateral triangle as shown in Fig. 1. The delta configuration proved to be the robust P-P based AVS configuration for the DOA estimation in the presence of noise (Wajid *et al.*, 2016), however, it gives a bias in the DOA estimate. Let the measured pressure signals at the three vertices of the delta configuration be $p_k(t)$, $p_l(t)$, and $p_m(t)$. The intensities along the dotted lines (in Fig. 1) are calculated using the method given in Sec. 2 and Eq. (12). These intensities are projected on the orthogonal axes. The average orthogonal intensity components are estimated by taking the average of the projected intensities on the corresponding orthogonal axes. Then using Eq. (13), the DOA estimate in 2D for the sinusoidal source of angular frequency ω_o is given by

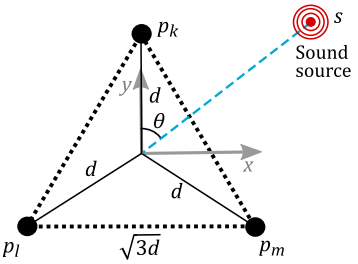

Fig. 1. Delta configuration, with three measured signals, i.e. p_k, p_l, and p_m. Darkened circles indicate the omni-directional microphone and S indicates the acoustic source in the far field.

$$\widehat{\theta}(\omega_o, d) = \tan^{-1}\left[\frac{x^* + y^*}{z^* + \sqrt{3}\sin(\omega_o \tau_{k,l})}\right], \tag{21}$$

where

$$x^* = \frac{2\sin(\omega_o \tau_{m,l})\,[1 - \kappa\tau_{k,l}\alpha(\omega_0, d)]}{[1 - \kappa\tau_{m,l}\alpha(\omega_0, d)]},$$

$$y^* = \left\{\sin(\omega_o \tau_{k,l}) - \frac{\sin\{\omega_o(\tau_{k,l} - \tau_{m,l})\}}{[1 - \kappa\tau_{m,l}\alpha(\omega_0, d)]}\right\},$$

$$z^* = \frac{\sqrt{3}\sin\{\omega_o(\tau_{k,l} - \tau_{m,l})\}}{[1 - \kappa\tau_{m,l}\alpha(\omega_0, d)]},$$

d is the microphone separation, as shown in Fig. 1, $\alpha(\omega, d)$ accounts for the signal strength loss due to absorption and spreading that depends on the angular frequency ω and d, which increases with increase in the frequency of the signal and decreases with increase in the microphone separation. The time delay of arrival $\tau_{i,j}$ between the i-th and j-th microphones for a planar wave propagating in the direction of the unit vector $\mathbf{a}$ is given by

$$\tau_{i,j} = \frac{\mathbf{a}^{\mathrm{T}}(\mathbf{r}_i - \mathbf{r}_j)}{\kappa}, \tag{22}$$

where $\mathbf{r}_i$ and $\mathbf{r}_j$ are the position vectors of the i-th and j-th microphones respectively, and κ is the speed of sound in air (Wajid *et al.*, 2016).

The analytical results of AE for various microphone separation d and DOAs are shown in Fig. 2. It shows that the AE (or bias) is a function of the microphone separation d and actual DOA, and it increases with increase in d excluding for few DOAs (0°, 60°, 120°, 180°, 240°, and 300°).

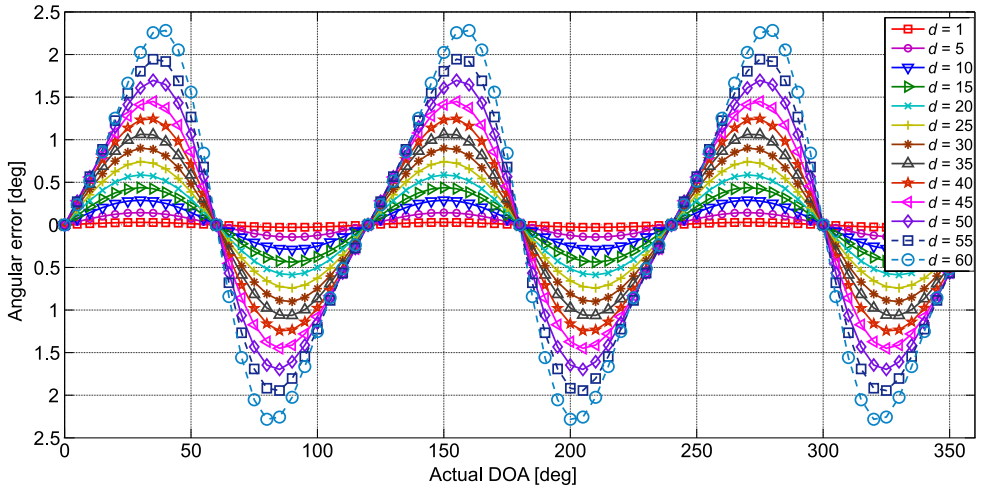

Fig. 2. Analytical results: AE versus DOAs for the sinusoidal source of 1 kHz with microphone separation d varied from 1 to 60 mm and the duration of the received signal is 25 ms.

Table 1. Analytical results: two components of AE, frequency dependent and frequency independent at $\theta = 30°$.

d [mm]	Frequency independent bias, AE [deg]	Frequency dependent bias, AE [deg]		
		F = 100 Hz	F = 500 Hz	F = 1 kHz
5	0.1436	3.0041e−06	7.5102e−05	3.0041e−04
15	0.4291	8.1111e−05	0.0020	0.0081
25	0.7032	3.7551e−04	0.0094	0.0376
35	0.9565	0.0010	0.0258	0.1030
45	1.1821	0.0022	0.0547	0.2190
55	1.3771	0.0040	0.1000	0.3998

To examine and quantify the effect of d and ω independently on angular error, the Maclaurin series expansion of the AE for Eq. (21) at a fixed DOA $\theta = 30°$ is given below:

$$\text{AE} \simeq \frac{90d}{\pi} + \frac{(45\sqrt{3}d^2)}{\pi} - \frac{5700d^3}{\pi} - \frac{(11475\sqrt{3}d^4)}{2\pi} + \frac{357138d^5}{\pi} + \frac{45\omega^2 d^3}{235298\pi}, \tag{23}$$

where d is in metres and AE is in degrees. Equation (23) gives a quantitative estimate of the bias introduced in the DOA estimate due to the microphone separation and the source signal frequency. This bias has two components, one is frequency dependent and the other is frequency independent. Table 1 gives the frequency dependent and frequency independent bias components for different frequencies with d varying from 5 mm to 55 mm. It shows that the frequency independent bias component is significantly larger than the frequency dependent bias component for all frequencies ranging from 100 Hz to 1 kHz, and these bias components increase with the increase in microphone separation. Also, the frequency dependent bias increases with d and ω. The bias of the DOA estimate can be easily reduced as it is a deterministic function of d and ω, thereby, the DOA estimate will get improved.

4. FEM simulation and proposed bias model for narrowband signal

4.1. FEM simulation and validation

To corroborate the analytical results of AE and its dependency on microphone separation and frequency, a Finite Element Method (FEM) tool, i.e. COMSOL Multiphysics, has been used to set up the experimental environment. The COMSOL Multiphysics is used to generate received signal at point size omni-directional microphones of an AVS. In this FEM simulation, the omni-directional acoustic source is kept at a distance of 1 m from the delta configured AVS, that acoustic source emits sinusoidal signal whose frequency is varied between 100 Hz to 1 kHz at intervals of 100 Hz. The angular location of the source is varied from 0° to 360° with increments of 5°. The signals are acquired at the omni-directional microphones of the AVS at a sampling rate of 48 kHz. The speed of sound κ is 343 m/s and the duration of the received signal is 25 ms. The AVS microphone signals are generated for different values of d (1 to 60 mm), for different frequencies of the source signal, and for different DOAs. The sample results for bias or AE are shown in Fig. 3. It has been observed that AE increases on increasing d for all the signal frequencies, excluding at a few DOAs (0°, 60°, 120°, 180°, 240°, and 300°). Also, there is a minor increase in the peak error on increasing the source signal frequency.

4.2. Bias model

The estimated DOA for the delta configuration is modified with the bias correction term in order to improve the DOA estimate. The bias corrected estimate $\widetilde{\theta}(\omega, d)$ for the delta configuration for narrowband signal centred at angular frequency ω, can be obtained by using

$$\widetilde{\theta}(\omega, d) = \widehat{\theta}(\omega, d) + \Delta\widehat{\theta}(\omega, d), \tag{24}$$

where the bias term, $\Delta\widehat{\theta}(\omega, d)$, is fitted with the sum of sines model as given below:

$$\Delta\widehat{\theta}(\omega, d) = \sum_{i=1}^{K} [a_i(\omega, d)\cos(\beta\theta) + b_i(\omega, d)\sin(\beta\theta)] + a_o, \tag{25}$$

and the model parameters $a_i(\omega, d)$, $b_i(\omega, d)$, and β are obtained after fitting the FEM simulated data (sample data is shown in Fig. 3) of AE with respect to the actual DOA for variable d and ω. A larger value of K would improve the parameter estimation accuracy, at the cost of more computations. The univariate (fixed frequency) and bivariate fitting polynomial models of bias are given below.

4.2.1. Univariate fitting polynomial model of bias

For a fixed frequency, $\omega_o = 2 \cdot 10^3\pi$ rad/s, the model parameters $a_1(\omega_o, d)$ and $b_1(\omega_o, d)$ are obtained,

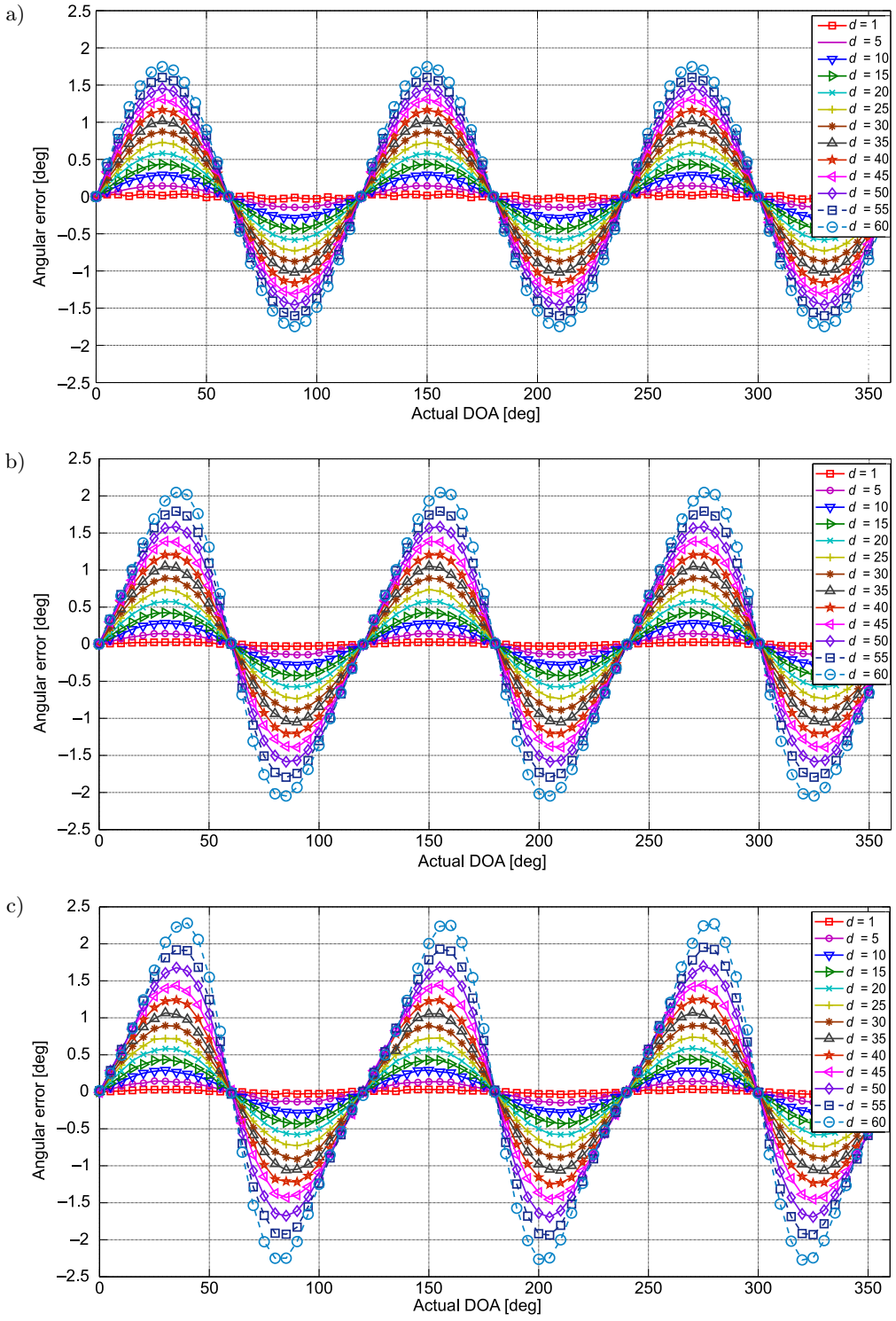

Fig. 3. FEM simulation results for AE versus DOAs for sinusoidal sources located at a range of 1 m with d varied from 1 to 60 mm and a signal duration of 25 ms. The sinusoidal signals frequency: a) F = 100 Hz, b) F = 900 Hz, and c) F = 1000 Hz. (*Note:* Results for other frequencies (200 Hz, 300 Hz, ..., 800 Hz) of the source signal are not shown due to space constraints).

thereby, $\Delta\widehat{\theta}(\omega_o, d)$ for $K = 1$. The parameters $a_1(\omega_o, d)$ and $b_1(\omega_o, d)$ are approximated using the fitting data of FEM simulation on the sum of sines model of Eq. (25) with R^2 (square of the correlation between the response values and the predicted response values) = 0.999, the approximated expressions are given by

$$b_1(d)|_{\text{at1 kHz}} = 134.5d^2 + 25.29d + 0.01549 \qquad (26)$$

and

$$a_1(d)|_{\text{at1 kHz}} = 7 - 2652d^3 + 124.3d^2 - 1.866d + 0.003512, \quad (27)$$

and $\beta = \pi/60$, a_o may be neglected as its value is of the order of 10^{-3}. The univariate fitted polynomials in Eqs (26) and (27) are of degree 2 and 3 respectively at frequency ω_o.

One may argue that the bias term, $\Delta\widehat{\theta}$, is a function of the unknown θ, but this can be addressed as follows. Let the actual DOA be 32.5° and the estimated DOA without bias correction be 31.609° (obtained from the linear interpolation of the DOA estimate simulated at 30° and 35°) at $d = 30$ mm, so we can correct the bias at 31.609° which is equal to 0.893°. If we include this correction, the estimated angle is 32.502° which is just 0.002° away from its true value. This small deviation may be due to interpolation and fitting error.

4.2.2. Bivariate fitting polynomial model of bias

In the above estimate of bias term, $\Delta\widehat{\theta}(\omega, d)$, the frequency ω is fixed at $\omega_o = 2 \cdot 10^3\pi$ rad/s. Now, consider the variable frequency, the parameters $a_i(d,\omega)$ and $b_i(d,\omega)$ are expressed in terms of both variables, i.e. ω and d. These parameters are obtained after fitting the FEM simulated data from 100 Hz to 1 kHz with an increment of 100 Hz on the sum of sines model of Eq. (25). The bivariate fitted polynomials are

$$b_1(d,\omega) = p_{b1}(\omega)d^2 + p_{b2}(\omega)d + p_{b3}(\omega) \quad (28)$$

and

$$a_1(d,\omega) = p_{a1}(\omega)d^3 + p_{a2}(\omega)d^2 + p_{a3}(\omega)d + p_{a4}(\omega), \quad (29)$$

where $p_{b1}(\omega)$, $p_{b2}(\omega)$, $p_{b3}(\omega)$, $p_{a1}(\omega)$, $p_{a2}(\omega)$, $p_{a3}(\omega)$, and $p_{a4}(\omega)$ are the polynomial in ω with degree 2 or 3.

In order to see the dependency of the bias term $\Delta\widehat{\theta}(d,\omega) = a_1(d,\omega)\cos(\beta\theta) + b_1(d,\omega)\sin(\beta\theta)$ on degrees of d and ω, the Maclaurin series expansion of $\Delta\widehat{\theta}(d,\omega)$ has been evaluated w.r.t. d and ω. This expansion helps us in distinguishing bias dependency on individual variables d and ω. The Macraulin series has been expanded up to 6 degrees of the polynomial, whose coefficients along with polynomial terms are given in Table 2. Looking into the polynomial coefficients from this table, it states that the bias dependency on the microphone separation is stronger than on the frequency variable. Also, the surface plots of the bias depicting the same have been shown in Figs 4 and 5. Consider the Eqs (30) and (31) obtained from Table 2 with $\theta = 30°$,

Table 2. The coefficients of Macraulin series expansion of the bias $\Delta\widehat{\theta}(\omega, d)$, where $\psi(\theta) = \sin(\beta\theta)$ and $\chi(\theta) = \cos(\beta\theta)$.

Term	Coefficient	Term	Coefficient
$d^0\omega^0$	$[-65\psi(\theta) + 1.21\chi(\theta)] \cdot 10^{-4}$	ω	$[55.62\psi(\theta) + 5.83\chi(\theta)] \cdot 10^{-7}$
d	$[26.65\psi(\theta) + 0.43\chi(\theta)] \cdot 10^{0}$	ω^2	$-[12.64\psi(\theta) + 3.20\chi(\theta)] \cdot 10^{-10}$
d^2	$[2.14\psi(\theta) - 34.07\chi(\theta)] \cdot 10^{0}$	ω^3	$[14.77\psi(\theta) + 4.99\chi(\theta)] \cdot 10^{-14}$
d^3	$[0\psi(\theta) + 558.2\chi(\theta)] \cdot 10^{0}$	$d\omega^2$	$[-2.16\psi(\theta) + 2.41\chi(\theta)] \cdot 10^{-7}$
$d\omega$	$[11.3\psi(\theta) - 6.20\chi(\theta)] \cdot 10^{-4}$	$d\omega^3$	$[0\psi(\theta) - 3.20\chi(\theta)] \cdot 10^{-11}$
$d^2\omega$	$[-4.34\psi(\theta) + 42.14\chi(\theta)] \cdot 10^{-3}$	$d^2\omega^2$	$[3.99\psi(\theta) - 16.5\chi(\theta)] \cdot 10^{-6}$
$d^3\omega$	$[\psi(\theta) - 7.4\chi(\theta)] \cdot 10^{1}$	$d^2\omega^3$	$[0\psi(\theta) + 2.20\chi(\theta)] \cdot 10^{-9}$
$d^3\omega^2$	$[\psi(\theta) + 2.98\chi(\theta)] \cdot 10^{-4}$	$d^3\omega^3$	$[0\psi(\theta) - 4.16\chi(\theta)] \cdot 10^{-8}$

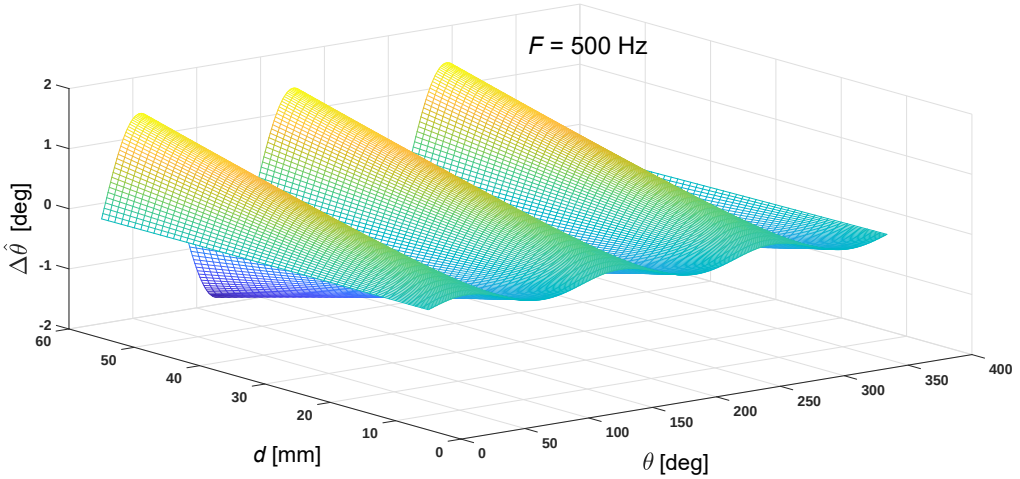

Fig. 4. Surface plot of the fitted $\Delta\widehat{\theta}$ with respect to d and θ at $F = 500$ Hz.

$$\Delta\widehat{\theta}(\omega, 5\text{ mm}) \approx 0.1268 + 1.1132 \cdot 10^{-5}\omega - 2.249 \cdot 10^{-9}\omega^2 - 2.249 \cdot 10^{-9}\omega^2 + 1.48 \cdot 10^{-13}\omega^3, \quad (30)$$

$$\Delta\widehat{\theta}(2 \cdot 10^3\pi, d) \approx 0.0152 + 25.2260d + 132.3920d^2 - 1.6072 \cdot 10^{-13}d^3. \quad (31)$$

It can be calculated and seen that the dependency of bias on frequency is small and it is more dependent on d.

Figures 6 and 7 show the variation of the AE w.r.t. frequency for different microphone separations. It is observed that the AE or bias is almost constant for

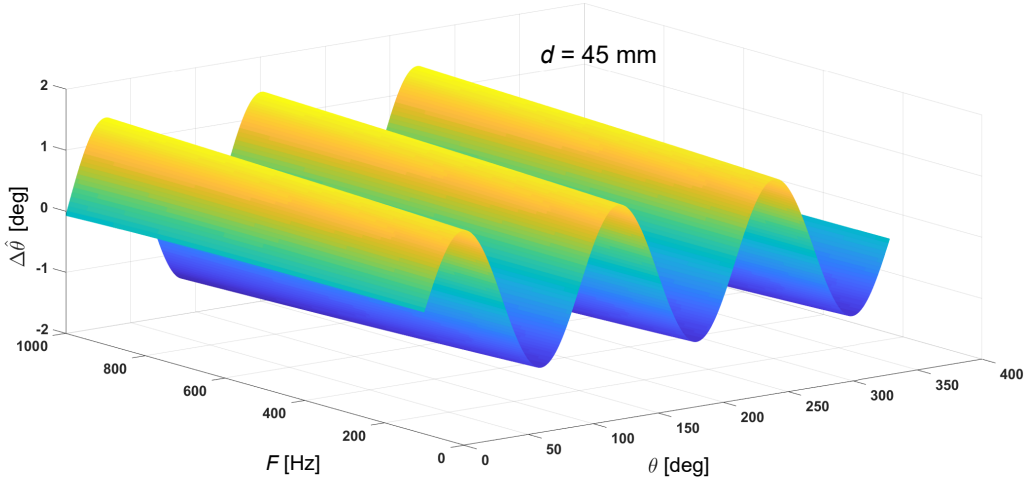

Fig. 5. Surface plot of the fitted $\Delta\widehat{\theta}$ with respect to F and θ at $d = 45$ mm.

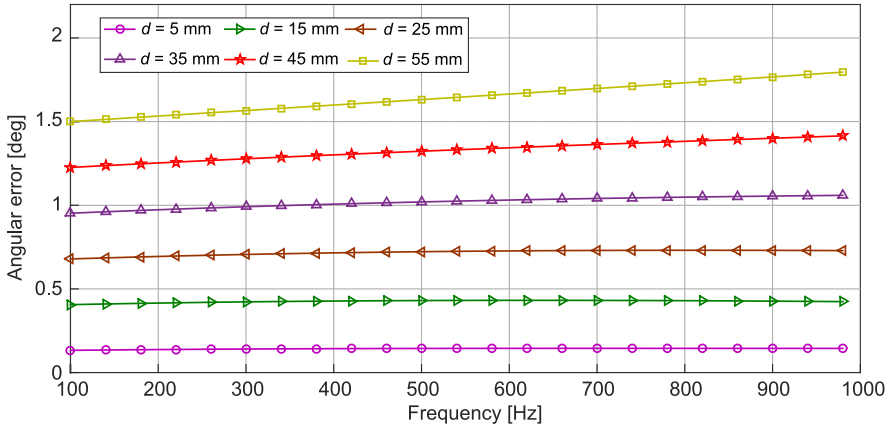

Fig. 6. FEM simulation results for AE versus frequency for different microphone separations d varied from 5 mm to 55 mm, the source is located at a range of 1 m at 30° and the source signal is of 25 ms duration.

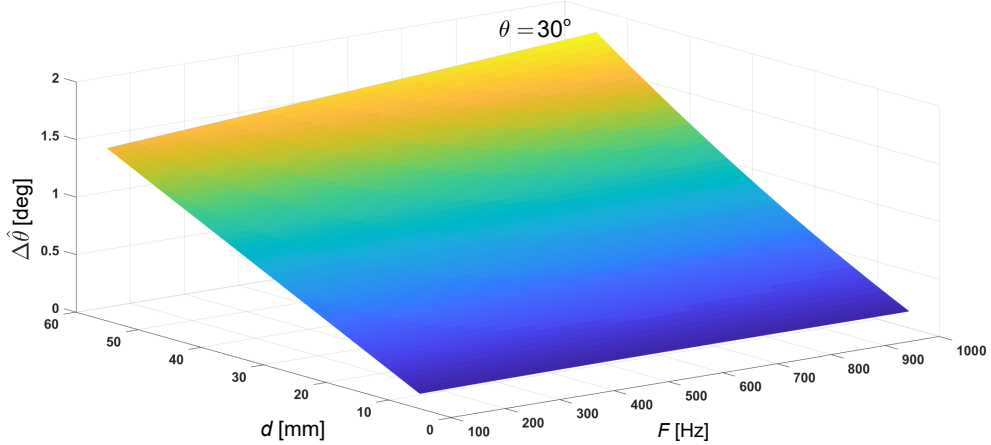

Fig. 7. Surface plot of the fitted $\Delta\widehat{\theta}$ with respect to d and F at $\theta = 30°$.

Table 3. FEM simulation: two components of AE, frequency dependent and frequency independent at $\theta = 30°$.

d [mm]	Frequency independent bias, AE [deg]	Frequency dependent bias, AE [deg]		
		F = 100 Hz	F = 500 Hz	F = 1 kHz
5	0.1268	0.0061	0.0174	0.0178
15	0.3937	0.0122	0.0368	0.0297
25	0.6611	0.0180	0.0614	0.0675
35	0.9289	0.0236	0.0911	0.1314
45	1.1971	0.0289	0.1259	0.2214
55	1.4657	0.0341	0.1659	0.3374

the frequency range from 100 to 1000 Hz for a smaller value of d (< 25 mm). As the value of d increases above 25 mm, the AE or $\Delta\widehat{\theta}$ becomes linearly dependent on signal frequency and the slope of this linear relation is proportional to d. For a fixed value of microphone separation, the bias is split into two components (frequency independent and frequency dependent), as given in Table 3. It is observed that the frequency dependent bias is much smaller than the frequency independent error, which corroborates with the analytical results given in Table 1. The possible reason for the minor mismatch of AE in the two tables (Tables 1 and 3) is due to the finite distance of the AVS from the source, finite signal duration, and curve fitting approximation with the sum of sines models for the FEM simulated data. The presented fitting model can be easily extended beyond the frequency range 100 to 1000 Hz, depending on the applications. Some results at 30° for 1500 Hz signal depicting true bias using COMSOL simulation and a bias calculated using the presented fitting model is shown in Table 4. It has seen observed that the true bias as well as calculated bias, are very close to each other.

Table 4. Bias results for 1500 Hz signal at 30°: true bias as per COMSOL simulation and a bias calculated using the presented fitting model.

d [mm]	True bias (COMSOL)	Bias calculated (model)
1	0.0262	0.0757
5	0.1439	0.1557
10	0.2972	0.2698
15	0.4474	0.3998
20	0.6195	0.5455
25	0.7954	0.707
30	0.9396	0.8843
35	1.1512	1.0774
40	1.3652	1.2862
45	1.5832	1.5109
55	2.1231	2.0075
60	2.4476	2.2795

4.3. Performance of bias correction schemes in the presence of noise

The ambient noise is generally correlated noise due to the closeness of the microphones in P-P based AVS configurations, whereas uncorrelated noise is due to sensor and electronic components which are independent of the microphone spacing. Therefore, the bias corrected estimate of DOA, as given in Eq. (24), and its performance are studied for different SNR values from 10 dB to 30 dB for both uncorrelated and correlated noise field. All DOA estimate results are presented after removal of 10% outliers obtained from 10,000 independent realisations of the omni-directional microphone signals in the noisy environment.

Figure 8 shows the RMSAE (on logarithmic scale) versus DOA for the uncorrelated noise field for different SNR values with different microphone separations. It has been seen that after removing the bias error from the estimator the reverse trend is observed, that is on increasing the microphone separation d the RMSAE decreases for all SNR values considered. This is due to the removal of bias, and the variance of DOA estimate being lower for larger d. The RMSAE comprises of two components, one is bias and the other is variance. The bias is an increasing function of microphone separation while variance is a decreasing function of microphone separation. When the microphones are closer, the direction of pressure gradient will have more ambiguity in the presence of noise due to lower SNR of the pressure difference signal that leads to higher variance of the DOA estimate. Figure 9 shows the $\overline{\text{RMSAE}}_{0°:15°:345°}$ versus microphone separation with error correction (without bias) as well as without error correction (with bias) in the presence of uncorrelated noise field and correlated noise field for different SNR values.

It is observed that the bias corrected DOA estimate performs much better for larger microphone separation and gives improved results even at lower SNR

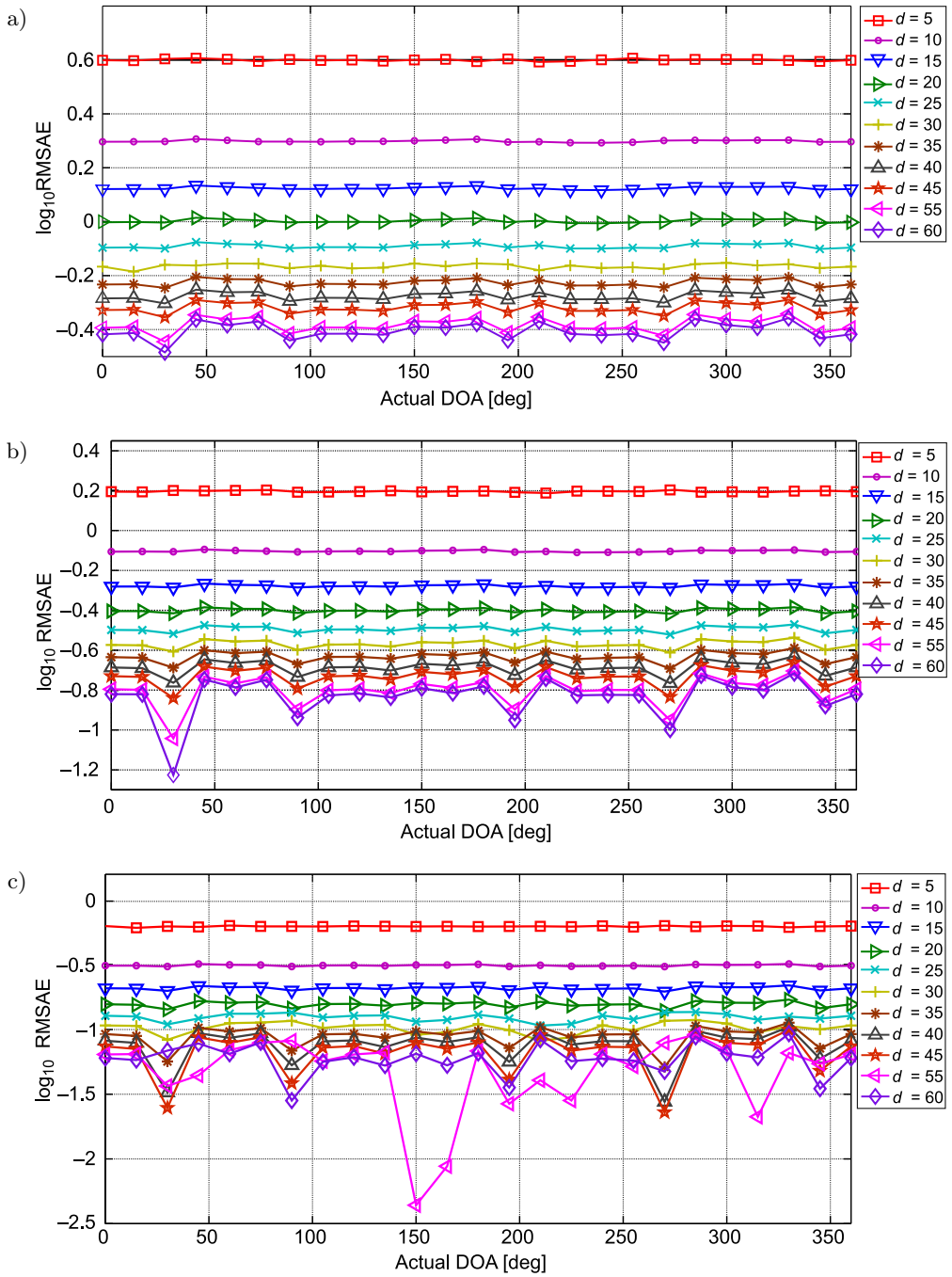

Fig. 8. RMSAE versus DOAs after bias correction when the acoustic source is at a range of 1 m and emits 1 kHz sinusoidal signal of 25 ms duration in the presence of uncorrelated noise field with: a) SNR = 10 dB, b) SNR = 18 dB, c) SNR = 26 dB. (*Note:* The vertical scales of all the graphs are different for better visualisation. Results for all values of SNR are not shown due to space constraints).

for uncorrelated as well as correlated noise field. At the larger microphone separation, the variance component is smaller than the bias component and hence the performance for larger microphone separation is better with bias correction. However, for lower microphone separation, the variance is relatively much higher than the bias so there is little improvement in performance after bias correction.

5. Proposed bias corrected DOA estimation algorithm for broadband signals

The bias correction method for the DOA estimate proposed in Sec. 4 is applicable for narrowband signals. In this section, bias correction technique is extended for broadband signals. We have devised a method for bias correction in DOA estimate for a broadband sig-

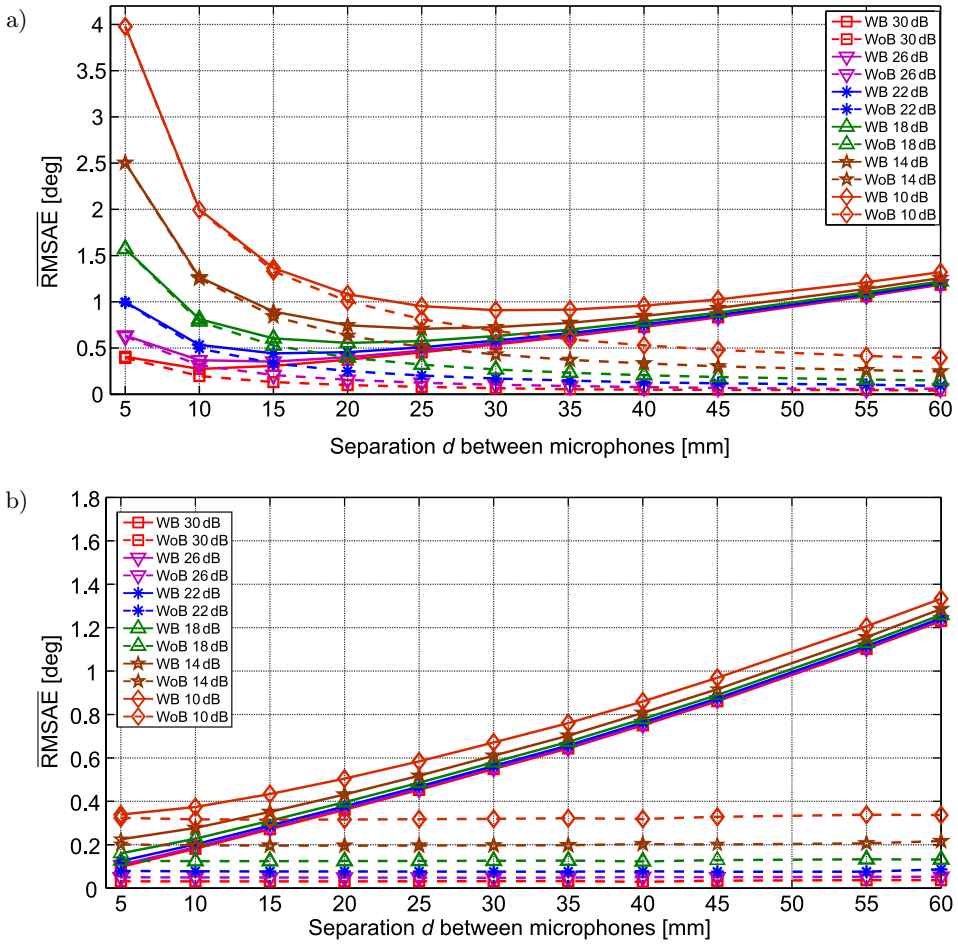

Fig. 9. $\overline{\text{RMSAE}}_{0°:15:345°}$ versus microphone separation d, before and after bias correction when an acoustic source is at a range of 1 m and emits 1 kHz sinusoidal signal of 25 ms duration in the presence of uncorrelated noise field (a) and correlated noise field (b), SNR varied from 30 dB to 10 dB with a decrement of 4 dB. (*Note:* WB indicates "with bias" and WoB indicates "without bias").

nal (example: speech source). The first step is to divide the received broadband signals at each microphone into 30 ms time frames and multiply these frames with a suitable window function such as a Hamming window. If the energy of the time frame is more than a set threshold, then determine the intensity spectrum components along the x-axis and y-axis. The intensities spectrum along the solid lines (Fig. 1) are calculated using the method given in Sec. 2 and Eq. (15). The orthogonal intensity components are estimated by taking the average of the projected intensities on the corresponding orthogonal axes. The orthogonal intensity spectrum components for delta configuration along x-axis and y-axis are given by

$$J_x(\omega) \triangleq +\frac{1}{3\sqrt{3}\rho_o d\omega}\text{Im}\left[S_{p_l p_m}(\omega)\right] + \frac{\sin(\phi)}{3\sqrt{3}\rho_o d\omega}\text{Im}\left[S_{p_k p_m}(\omega)\right] + \frac{\sin(\phi)}{3\sqrt{3}\rho_o d\omega}\text{Im}\left[S_{p_l p_k}(\omega)\right] \tag{32}$$

and

$$J_y(\omega) \triangleq +\frac{\cos(\phi)}{3\sqrt{3}\rho_o d\omega}\text{Im}\left[S_{p_k p_m}(\omega)\right] + \frac{\cos(\phi)}{3\sqrt{3}\rho_o d\omega}\text{Im}\left[S_{p_k p_l}(\omega)\right], \tag{33}$$

respectively. Further, the peak for the intensity spectrum component and its frequency index are determined. Based on the peak value obtained, all frequency indices such that the intensity spectrum components value is more than a threshold are identified. For the peak frequency index and other identified frequency indices, we estimate the DOAs and apply the narrow band bias corrections scheme as described in Sec. 4. For the speech signal, the peak frequency will always lie within the frequency range of 100 to 1000 Hz. The detailed steps for the bias correction in DOA estimation for a broadband signal are given in Algorithm.

The FEM simulation results for DOA estimation without and with bias correction of speech source DOA for two different microphone separations are given in Fig. 10. For d = 10 mm, $\overline{\text{AAE}}_{0°:5°:60°}$ is 0.173° before

Algorithm. Bias correction in DOA estimate for speech signal using delta configuration.

1) Let the received signals of omni-directional microphones at an AVS be $p_k(n)$, $p_l(n)$, and $p_m(n)$, where $0 \le n < N$. These signals are broadband signals recorded at the AVS.
2) Segment each received signals into N_o number of samples and multiply each segment with Hamming window $\forall\ n = 0, 1, 2, ..., N_o - 1$ and $r = 0, 1, 2, ..., N/N_o - 1$

$$p_z^r(n) = p_k(n + rN)\left[0.54 - 0.46\cos\left(2\pi\frac{n}{N_o - 1}\right)\right] \quad \forall\ z \in \{k, l, m\}.$$

3) Repeat for every $r = 0, 1, 2, ..., N/N_o - 1$:
   if $E\,(p_k^r(n)) > \gamma$, calculate the intensity spectrum components $J_x(\omega)$ and $J_y(\omega)$ along x-axis and y-axis, respectively, as given by Eqs (32) and (33)
   (a) Find peak of the absolute of $J_x(\omega)$ and $J_y(\omega)$
      (i) $\{\Lambda_x, i_x\} = \max\{\text{abs}(J_x^r(\omega)), \epsilon\}$
      (ii) $\{\Lambda_y, i_y\} \max\{\text{abs}(J_y^r(\omega)), \epsilon\}$,
      where ϵ is the threshold for peak in the intensity spectrum components; Λ_x and i_x contains the peak and its index. Assume $\mathbf{i} = i_x \cup i_y$.
   (b) $\{\Upsilon_x(\omega) = \text{abs}(J_x^r(\omega))\} \wedge \{\Upsilon_y(\omega) = \text{abs}(J_y^{r,}(\omega))\}$
      $\forall\ \{\omega \,|\, \text{abs}(J_x^r(\omega)) > \max\{\text{abs}(J_x^r(i))\}/4\}$
   (c) $\widetilde{\theta}(\omega) = \tan^{-1}\frac{\Upsilon_x(\omega)}{\Upsilon_y(\omega)} + \Delta\widetilde{\theta}(\omega, d)$
   (d) $\widetilde{\theta}^r_{\text{avg}} = \underset{\omega}{\text{average}}\left\{\widetilde{\theta}(\omega)\right\}$
4) $\widetilde{\theta} = \underset{r}{\text{avg}}\left\{\widetilde{\theta}^r_{\text{avg}}\right\} \forall \left\{r : \text{outliers of } \widetilde{\theta}^r_{\text{avg}} \text{ are removed}\right\}$

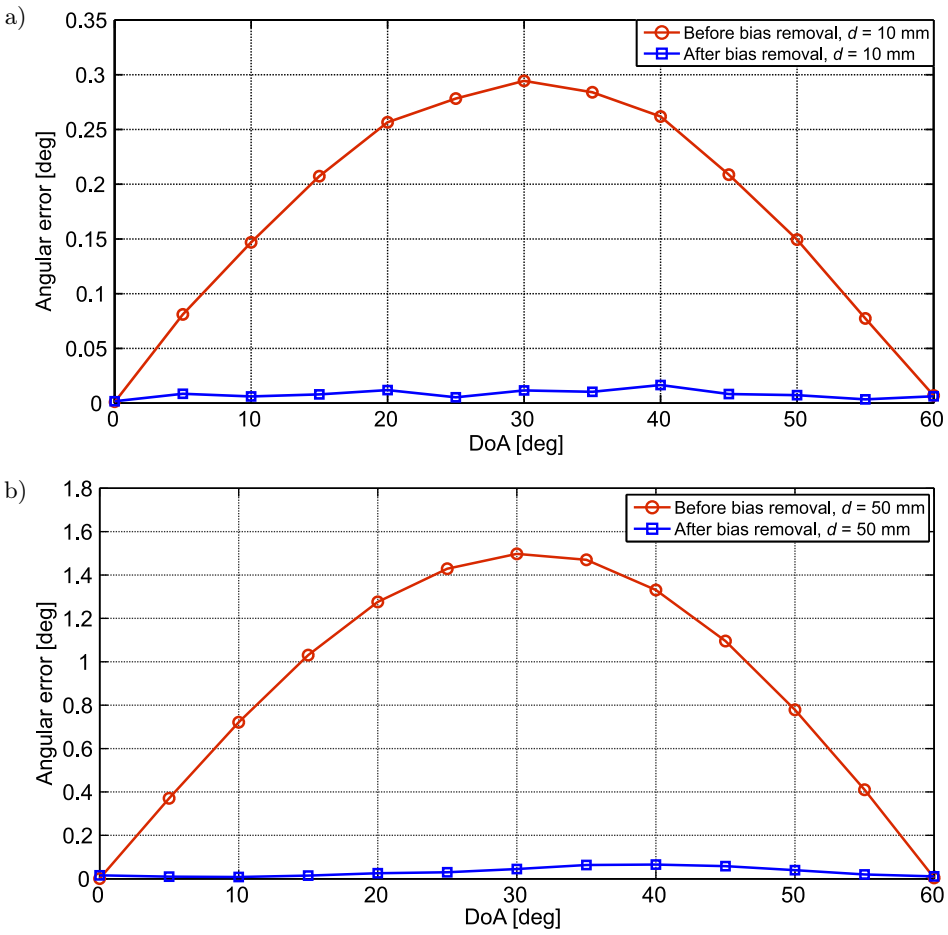

Fig. 10. Angular error (AE) versus actual DOA, showing error before bias correction and after bias correction for speech source of 3 s duration at a range of 1 m: a) d = 10 mm, b) d = 50 mm. (*Note:* The vertical scales of the two graphs are different for better depiction).

bias correction and $\overline{\text{AAE}}_{0°:5°:60°}$ is 0.008° after bias correction. For d = 50 mm, $\overline{\text{AAE}}_{0°:5°:60°}$ is 0.878° before bias correction and $\overline{\text{AAE}}_{0°:5°:60°}$ is 0.030° after bias correction.

6. Experiment in an anechoic environment

In this section, we experimentally study the effect of microphone separation on the DOA estimate and apply the proposed bias correction to the DOA estimate. The delta configuration of an AVS is fabricated using three identical omni-directional microphones (model: MKE-1, make: Sennheiser Germany). These microphones are of diameter 3.3 mm and have sensitivity of 5 mV/Pa at 1 kHz. The microphone fixture shown in Fig. 11 is fabricated using high-resolution 3D printer with Polylactic Acid (PLA) thermoplastic printing material. This microphone fixture allows the microphone separation d to be varied from 15 mm to 55 mm with increments of 10 mm. The microphones can be mounted on the tips of the three rods of this fixture. The acoustic full anechoic room ($2.06 \times 3.04 \times 3.34$ m dimensions) is used to perform the experiment in order to avoid reflections from the surroundings with instrument controls from outside the anechoic room. The signals acquired by the microphone are given to the preamplifier and the amplified signals are digitised with a sampling rate of 48 kHz. The loudspeaker (M-Audio A V-40) is used to generate a sound signal of 1 kHz of 1 s duration at a distance of 1 m from the AVS. The experiment is performed for DOA ranging from 0° to 60° with intervals of 5°. The DOA is estimated using Eq. (21). Figure 12 shows the AE versus actual DOA for different values of d which also include bias. It is observed that with the increase in d, the AE increases for a fixed angular location. Upon comparing the AE results with the simulation results, it is clear that experimental results show more deviation from the true DOA. However, the trend of increase in error with d is

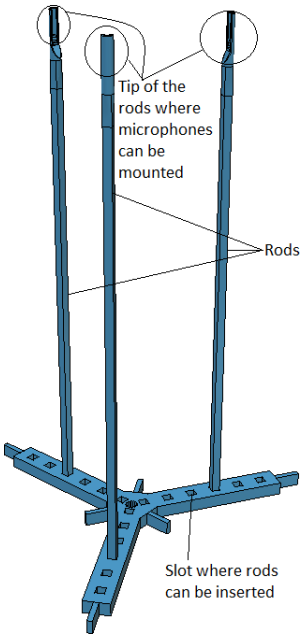

Fig. 11. Microphone fixture, with reconfigurable microphone separation d. This fixture has several slots in its base where rods holding microphones can be inserted with different separation.

clearly observed from the experimental results, as was the case with simulation results. The results of AE after removal of bias using the proposed technique are shown in Fig. 13, which shows the significant improvement in the DOA estimate. The higher value of AE for the experimental results relative to simulation may be due to the practical considerations of the finite size of microphones, diffraction and reflections from the microphone fixture, the finite size of the acoustic source, phase mismatch between the microphones, instrument and sensor noise, microphone placement error, etc. Figure 14 shows the $\overline{\text{AAE}}_{0°:5°:60°}$ versus d for the experiment which depicts the reduction in the average error after the bias correction.

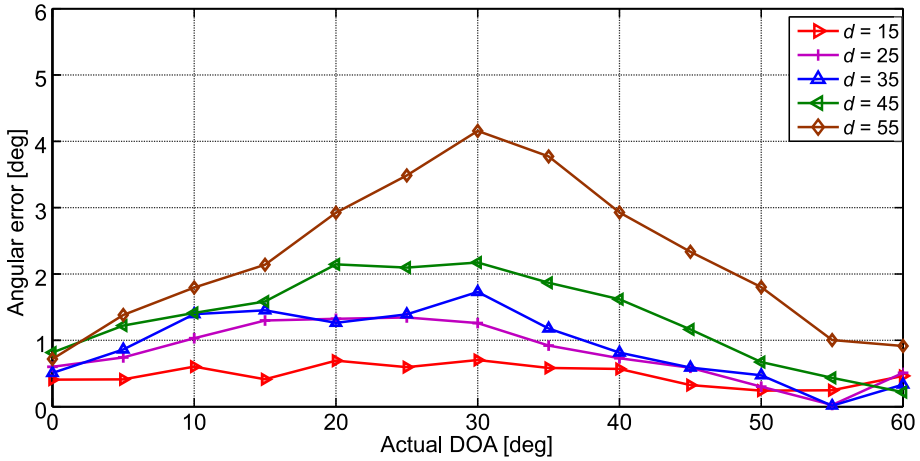

Fig. 12. AE [deg] versus microphone separation d before bias correction, when acoustic source is at a range of 1 m and emits 1 kHz sinusoidal signal of 1 s duration in the acoustic full-anechoic room.

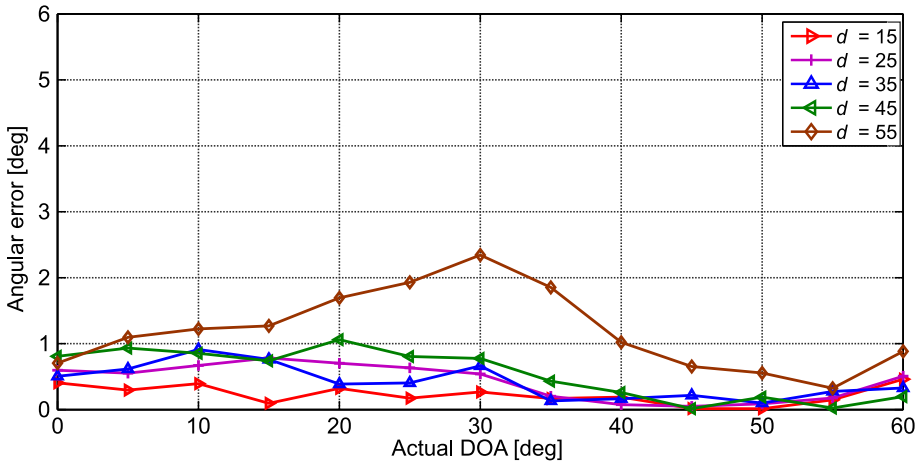

Fig. 13. AE [deg] versus microphone separation d after bias correction, when the acoustic source is at a range of 1 m and emits 1 kHz sinusoidal signal of 1 s duration in the acoustic full anechoic room.

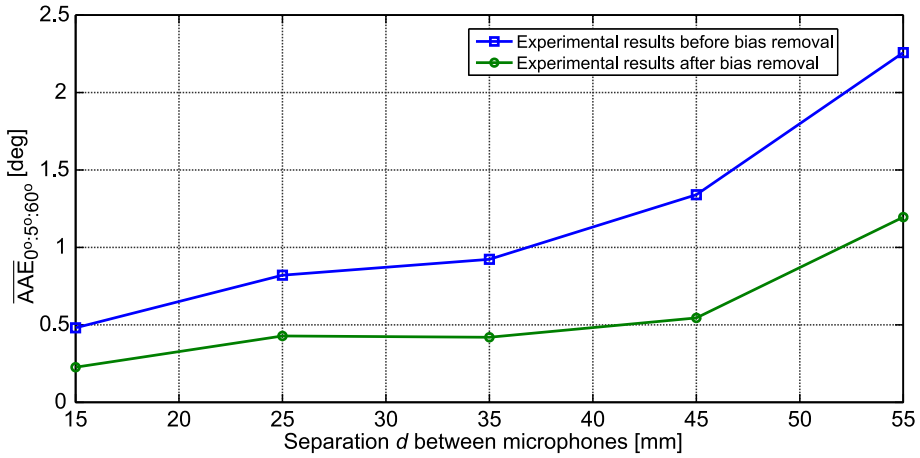

Fig. 14. $\overline{\mathrm{AAE}}_{0°:5°:60°}$ [deg] versus microphone separation d when the sound source is at a range of 1 m and emits 1 kHz sinusoidal signal of 1 s duration in the acoustic full anechoic room (experimental results before bias correction and experimental results after bias correction).

7. Conclusion

The bias in the DOA estimate caused due to microphone separation in an AVS and signal frequency has been quantified using a model fitting. The proposed bias correction schemes for the narrownband and broadband signals have been applied to the DOA estimate. The simulation results of frequency dependent and frequency independent bias are validated by the analytical results. The less dependence of angular error on the signal frequency causes that it is almost independent of the frequency for microphone separation less than 25 mm. Also, the bias is almost linearly proportional to the microphone separation (>25 mm) for frequency below 1 kHz. It is shown that at large microphone separation the bias corrected DOA estimator performs better than the uncorrected DOA estimator even at small SNR. The variance of the DOA estimate due to noise is reduced by increasing the microphone separation and then applying the proposed bias correction. The DOA estimate of the broadband signal is studied and the bias correction algorithm is applied to the DOA estimate of a speech source which results in a notable improvement in the DOA accuracy. The experiments in the acoustic anechoic room supported our simulation study of the proposed bias correction of the DOA estimate. In the future, the proposed scheme can be extended for the bias correction of the range estimate in the near field and for the bias correction in the presence of an interfering source with variable energy.

References

1. Bai M., Juan S.-W., Chen C.-C. (2013), Particle velocity estimation based on a two-microphone array and Kalman filter, *The Journal of the Acoustical Society of America*, **133**(3): 1425–1432, doi: 10.1121/1.4788986.
2. Cazzolato B.S., Hansen C.H. (2000), Errors in the measurement of acoustic energy density in one-dimen-

sional sound fields, *Journal of Sound and Vibration*, **236**(5): 801–831, doi: 10.1006/jsvi.2000.3002.

3. Chung J. (1978), Cross-spectral method of measuring acoustic intensity without error caused by instrument phase mismatch, *The Journal of the Acoustical Society of America*, **64**(6): 1613–1616, doi: 10.1121/1.382145.
4. Dall'Osto D.R., Dahl P.H. (2015), Using vector sensors to measure the complex acoustic intensity field, *The Journal of the Acoustical Society of America*, **138**(3): 1767–1767, doi: 10.1121/1.4933587.
5. de Bree H.-E. (2003), An overview of microflown technologies, *Acta Acustica United with Acustica*, **89**(1): 163–172.
6. de Bree H.-E., Druyvesteyn E., Raangs R. (2001), A low cost intensity probe, [in:] *Audio Engineering Society Convention*, Paper 5292, http://www.aes.org/e-lib/browse.cfm?elib=9971.
7. Fahy F.J. (1977), Measurement of acoustic intensity using the cross-spectral density of two microphone signals, *The Journal of the Acoustical Society of America*, **62**(4): 1057–1059, doi: 10.1121/1.381601.
8. Gade S. (1982), Sound Intensity (Theory), *Technical Review to Advance Techniques in Acoustical, Electrical and Mechanical Measurements*, Bruel & Kjær, DK-2850 NAERUM Offset, Denmark, No. 3.
9. Giraud J.H., Gee K.L., Ellsworth J.E. (2010), Acoustic temperature measurement in a rocket noise field, *The Journal of the Acoustical Society of America*, **127**(5): EL179–EL184, doi: 10.1121/1.381601.
10. Hickling R., Brown A. (2011), Determining the direction to a sound source in air using vector sound-intensity probes, *The Journal of the Acoustical Society of America*, **129**(1): 219–224, doi: 10.1121/1.3518754.
11. Jacobsen F. (2007), Sound intensity measurements, [in:] *Handbook of Noise and Vibration Control*, Crocker M.J. [Ed.], John Wiley & Sons: Hoboken, New Jersey, Ltd, pp. 534–548, doi: 10.1002/9780470209707.ch45.
12. Jacobsen F. (2014), Sound intensity, [in:] *Springer Handbook of Acoustics*, *Springer Handbooks*, Rossing T.D. [Ed.], pp. 1093–1114, Springer: New York, NY, doi: 10.1007/978-1-4939-0755-7_25.
13. Jacobsen F., Cutanda V., Juhl P.M. (1998), A numerical and experimental investigation of the performance of sound intensity probes at high frequencies, *The Journal of the Acoustical Society of America*, **103**(2): 953–961, doi: 10.1121/1.421212.
14. Jacobsen F., de Bree H.-E. (2005), A comparison of two different sound intensity measurement principles, *The Journal of the Acoustical Society of America*, **118**(3): 1510–1517, doi: 10.1121/1.1984860.
15. Kotus J. (2012), Multiple sound sources localization in real time using acoustic vector sensor, *Communications in Computer and Information Science – Multimedia Communications, Services and Security*, **287**: 168–179, doi: 10.1007/978-3-642-30721-8_17.
16. Kotus J. (2015), Multiple sound sources localization in free field using acoustic vector sensor, *Multimedia Tools and Applications*, **74**(12): 4235–4251, doi: 10.1007/s11042-013-1549-y.
17. Kotus J., Czyżewski A. (2010), Acoustic radar employing particle velocity sensors, *Advances in Multimedia and Network Information System Technologies*, **80**: 93–103, doi: 10.1007/978-3-642-14989-4_9.
18. Kotus J., Czyżewski A., Kostek B. (2016), 3D acoustic field intensity probe design and measurements, *Archives of Acoustics*, **41**(4): 701–711, doi: 10.1515/aoa-2016-0067.
19. Kotus J., Kostek B. (2015), Measurements and visualization of sound intensity around the human head in free field using acoustic vector sensor, *Journal of the Audio Engineering Society*, **63**(1/2): 99–109, doi: 10.17743/jaes.2015.0009.
20. Kotus J., Lopatka K., Czyżewski A. (2014), Detection and localization of selected acoustic events in acoustic field for smart surveillance applications, *Multimedia Tools and Applications*, **68**(1): 5–21, doi: 10.1007/s11042-012-1183-0.
21. Lee C.H., Lee H.R.L., Wong K.T., Razo M. (2016), The spatial-matched filter beam pattern of a biaxial non-orthogonal velocity sensor, *Journal of Sound and Vibration*, **367**: 250–255, doi: 10.1016/j.jsv.2015.12.046.
22. Miah K.H., Hixon E.L. (2010), Design and performance evaluation of a broadband three dimensional acoustic intensity measuring system, *The Journal of the Acoustical Society of America*, **127**(4): 2338–2346, doi: 10.1121/1.3327508.
23. Odya P., Kotus J., Szczodrak M., Kostek B. (2017), Sound intensity distribution around organ pipe, *Archives of Acoustics*, **42**(1): 13–22, doi: 10.1515/aoa-2017-0002.
24. Olenko A., Wong K.T. (2015), Noise statistics across the three axes of a tri-axial velocity sensor constructed of pressure sensors, *IEEE Transactions on Aerospace and Electronic Systems*, **51**(2): 843–852, doi: 10.1109/TAES.2014.140242.
25. Olenko A.Y., Wong K.T. (2013), Noise statistics of a higher order directional sensor, realized by computing finite differences spatially across multiple isotropic sensors, *IEEE Transactions on Aerospace and Electronic Systems*, **49**(4): 2792–2798, doi: 10.1109/TAES.2013.6621854.
26. Parkins J.W., Sommerfeldt S.D., Tichy J. (2000), Error analysis of a practical energy density sensor, *The Journal of the Acoustical Society of America*, **108**(1): 211–222, doi: 10.1121/1.429458.
27. Raangs R., Druyvesteyn W., De Bree H. (2003), A low-cost intensity probe, *Journal of the Audio Engineering Society*, **51**(5): 344–357, http://www.aes.org/e-lib/browse.cfm?elib=12225.
28. Shi J. (2015), DOA estimation for arbitrary four-sensor array configurations based on three-dimensional sound intensity measurement, *International Journal of Applied Mathematics & Information Sciences*, **9**(2): 899–905, 10.12785/amis/090238.

29. Shirahatti U., Crocker M.J. (1992), Two-microphone finite difference approximation errors in the interference fields of point dipole sources, *The Journal of the Acoustical Society of America*, **92**(1): 258–267, doi: 10.1121/1.404289.

30. Song Y., Li Y.L., Wong K.T. (2015), Acoustic direction finding using a pressure sensor and a uniaxial particle velocity sensor, *IEEE Transactions on Aerospace and Electronic Systems*, **51**(4): 2560–2569, doi: 10.1109/TAES.2015.130837.

31. Song Y., Wong K.T. (2015), Acoustic direction finding using a spatially spread tri-axial velocity sensor, *IEEE Transactions on Aerospace and Electronic Systems*, **51**(2): 834–842, doi: 10.1109/TAES.2014.130320.

32. Song Y., Wong K.T., Li Y. (2015), Direction finding using a biaxial particle-velocity sensor, *Journal of Sound and Vibration*, **340**: 354–367, doi: 10.1016/j.jsv.2014.11.027.

33. Thomas D.C., Christensen B.Y., Gee K.L. (2015), Phase and amplitude gradient method for the estimation of acoustic vector quantities, *The Journal of the Acoustical Society of America*, **137**(6): 3366–3376, doi: 10.1121/1.4914996.

34. Thompson J., Tree D. (1981), Finite difference approximation errors in acoustic intensity measurements, *Journal of Sound and Vibration*, **75**(2): 229–238, doi: 10.1016/0022-460X(81)90341-2.

35. Wajid M., Kumar A. (2020), Direction estimation and tracking of coherent sources using a single acoustic vector sensor, *Archives of Acoustics*, **45**(2): 209–219, doi: 10.24425/aoa.2020.132495.

36. Wajid M., Kumar A., Bahl R. (2016), Design and analysis of air acoustic vector-sensor configurations for two-dimensional geometry, *The Journal of the Acoustical Society of America*, **139**(5): 2815–2832, doi: 10.1121/1.4948566.

37. Wiederhold C.P., Gee K.L., Blotter J.D., Sommerfeldt S.D. (2012), Comparison of methods for processing acoustic intensity from orthogonal multimicrophone probes, *The Journal of the Acoustical Society of America*, **131**(4): 2841–2852, doi: 10.1121/1.3692242.

38. Wiederhold C.P., Gee K.L., Blotter J.D., Sommerfeldt S.D., Giraud J.H. (2014), Comparison of multimicrophone probe design and processing methods in measuring acoustic intensity, *The Journal of the Acoustical Society of America*, **135**(5): 2797–2807, doi: 10.1121/1.4871180.

39. Wong K.T., Zoltowski M.D. (1997), Extended-aperture underwater acoustic multisource azimuth/elevation direction-finding using uniformly but sparsely spaced vector hydrophones, *IEEE Journal of Oceanic Engineering*, **22**(4): 659–672, doi: 10.1109/48.650832.

40. Zoltowski M.D., Wong K.T. (2000), Closed-form eigenstructure-based direction finding using arbitrary but identical subarrays on a sparse uniform cartesian array grid, *IEEE Transactions on Signal Processing*, **48**(8): 2205–2210, doi: 10.1109/78.852001.